Environmental Science Nano

ROYAL SOCIETY OF CHEMISTRY

PAPER

View Article Online
View Journal | View Issue

Cite this: *Environ. Sci.: Nano*, 2025, 12, 1965

Designing safer nanohybrids: stability and ecotoxicological assessment of graphene oxide–gold nanoparticle hybrids in embryonic zebrafish†

Bashiru Ibrahim,* Taiwo Hassan Akere, Pankti Dhumal, Eugenia Valsami-Jones and Swaroop Chakraborty *

Graphene oxide (GO) and graphene oxide–gold (GO–Au) nanohybrids offer promising applications in nanomedicine, biosensing, and environmental technology due to their unique properties. However, concerns regarding their environmental and biological safety remain largely unexplored. This study, using a safe and sustainable by design (SSbD) approach, evaluates the cytotoxicity, oxidative stress, and dispersion stability of GO and GO–Au nanohybrids in zebrafish ZF4 cells. GO was synthesised using a modified Hummer's method and GO–Au nanohybrids were prepared by incorporating gold nanoparticles (AuNPs) into the GO matrix. Physicochemical characterisation revealed enhanced dispersion stability of GO–Au nanohybrids, retaining over 98% of their initial absorbance in ultrapure water (UPW) and over 95% in DMEM/F12 after 48 hours. In contrast, GO displayed higher levels of sedimentation. Toxicity assessments indicated a dose- and time-dependent decrease in cell viability. After 72 hours, ZF4 cell viability was reduced to 39.5% for 150 μg mL^{-1} GO, whereas GO–Au treatment at the same concentration exhibited a less severe reduction (54.5% viability). Reactive oxygen species (ROS) generation was significantly higher in GO-treated cells compared to GO–Au, with GO generating approximately 2x more ROS at concentrations of 50 μg mL^{-1} and 100 μg mL^{-1}. Apoptosis and necrosis rates were also significantly elevated in GO-treated cells, with necrosis reaching 53.1% at 100 μg mL^{-1}, compared to 14.6% in GO–Au-treated cells. These findings demonstrate that the incorporation of AuNPs reduces cytotoxicity and oxidative stress by enhancing the colloidal stability of GO–Au nanohybrids. This study provides critical baseline data on the interaction of GO-based nanomaterials (NMs) with biological systems and highlights the importance of NM modification for safer, more sustainable applications.

Received 15th December 2024,
Accepted 17th January 2025

DOI: 10.1039/d4en01173b

rsc.li/es-nano

Environmental significance

This study addresses a critical gap in understanding the environmental and biological safety of graphene oxide (GO) and graphene oxide–gold (GO–Au) nanohybrids, materials widely explored for environmental and biomedical applications. By adopting a safe and sustainable by design (SSbD) approach, we demonstrate that incorporating gold nanoparticles into GO reduces cytotoxicity, oxidative stress, and aggregation, enhancing the overall stability of nanohybrids in biological environments. This research provides vital insights into the nanoscale interactions of GO-based materials with living systems, offering strategies to mitigate environmental risks associated with their use. The findings support the design of safer nanomaterials for environmental applications such as pollutant remediation, biosensing, and drug delivery, contributing to the responsible development of nanotechnology for sustainable use.

1. Introduction

Graphene oxide (GO) is a two-dimensional NM composed of carbon atoms arranged in a hexagonal lattice, functionalised with oxygen-containing groups.[1] This unique structure endows GO with exceptional properties such as high thermal stability, electrical conductivity, mechanical strength, and chemical versatility, making it widely applicable in materials science, nanomedicine, and environmental technology.[2,3] Additionally, its large surface area allows GO to serve as an ideal platform for the creation of nanohybrid NMs that combine distinct properties to produce enhanced or novel functionalities.[4] One promising example is graphene oxide–gold (GO–Au) nanohybrids, which have demonstrated significant potential in fields such as biosensing and cancer therapy.[5] However, despite their growing application, the environmental and biological safety of GO and its hybrids remains largely unexplored, raising concerns about their long-term effects on human health and ecosystems.

School of Geography, Earth & Environmental Sciences, University of Birmingham, Edgbaston, UK. E-mail: b.ibrahim@bham.ac.uk, s.chakraborty@bham.ac.uk

† Electronic supplementary information (ESI) available. See DOI: https://doi.org/10.1039/d4en01173b

Given the expanding use of 2D materials like GO, understanding their internalisation, interactions, and fate within biological systems is critical to assessing their safety.[6,7] GO's large surface area and reactive surface functional groups enable it to interact with biomolecules such as proteins, lipids, and nucleic acids, leading to

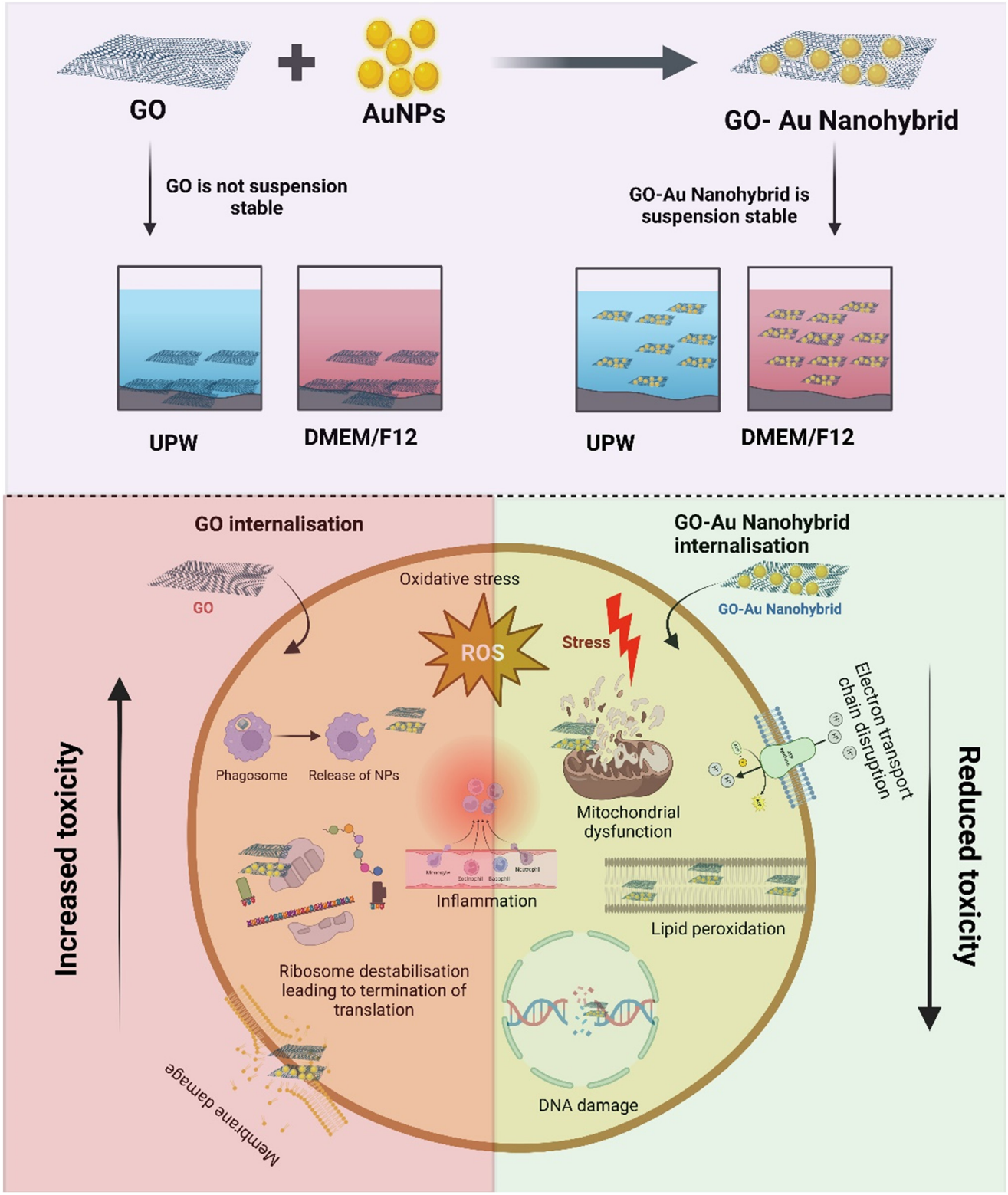

Scheme 1 Schematic showing GO's poor suspension stability and higher toxicity due to oxidative stress, inflammation, and DNA damage, while GO–Au nanohybrids exhibit improved stability and reduced toxicity through gold nanoparticle incorporation (schematic prepared using Biorender Software).

biological effects like oxidative stress and cell death.[8,9] These interactions are influenced by factors such as surface chemistry, functionalisation, and particle size, which in turn affect its ability to penetrate cellular barriers and its biodistribution.[10] The potential risks associated with GO and GO–Au nanohybrids highlight the need for rigorous safety assessments that explore their interactions with biological systems, particularly in relation to cytotoxicity and cellular uptake.[11,12]

Our study addresses these gaps by investigating the safety of GO–Au nanohybrids using the zebrafish ZF4 cell line—a model system widely recognised for its relevance in ecotoxicological and toxicological research. Zebrafish models, due to their genetic similarities to mammals, have become invaluable for studying the biological effects of NMs and environmental pollutants.[13–15] The ZF4 cell line, derived from zebrafish embryos, offers a high-throughput, *in vitro* alternative to animal studies, enabling efficient evaluation of NM toxicity.[16,17]

Our research adopts the safe and sustainable by design (SSbD) framework, as outlined by the European Commission, which aims to minimise risks and maximise sustainability by integrating safety considerations into the early stages of material development.[18] By focusing on *e.g.*, reducing toxicity or improving environmental compatibility, this study demonstrates how the SSbD framework can be applied to GO while achieving reduced toxicity throughout the lifecycle of the materials for various applications. By focusing on cytotoxicity, oxidative stress, and cell death pathways, this study provides critical insights into the interactions between GO–Au nanohybrids and biological systems.[19]

The novelty of this work lies in its use of ZF4 cells to systematically assess the nanosafety of GO–Au nanohybrids, contributing to the development of safer NMs. The findings will not only inform the design of safer GO–Au hybrids but also advance our understanding of their biological impacts, thus promoting the responsible use of nanotechnology in environmental and biomedical applications (Scheme 1).

2. Experimental section

2.1 Materials

Graphite flakes, sodium nitrate ($NaNO_3$), sulfuric acid (H_2SO_4, 98% w/w), potassium permanganate ($KMnO_4$), hydrogen peroxide (H_2O_2, 30% w/w), chloroauric acid ($HAuCL_4$), tannic acid ($C_{76}H_{52}O_{46}$), trisodium citrate ($Na_3C_6H_5O_7$) and dimethyl sulfoxide were procured from Sigma Aldrich (Dorset, UK). Phosphate-buffered saline (PBS), DMEM/F12, phenol-free RPMI 1640, penicillin/streptomycin, 0.25% trypsin–EDTA, a CellROX Deep Red reagent kit and an Alexa Fluor 488 annexin V/PI dead cell kit were purchased from Thermo Fisher Scientific (Paisley, UK). All the chemicals and reagents used in performing the experiments are of analytical grade.

2.2 GO synthesis

GO was synthesised using a modified version of Hummer's method.[20] Briefly, 5.0 g of graphite flakes, 3.75 mg of $NaNO_3$, and 370 mL of H_2SO_4 were combined in a 1 L twin-neck round bottom flask under magnetic stirring at room temperature. After 10 minutes of stirring, the mixture was cooled in an ice bath for 10 more minutes. Then, 22.5 g of $KMnO_4$ was slowly added while stirring, turning the mixture into a dark green paste. Stirring continued for 72 hours at room temperature in a fume hood. The mixture was diluted with 500 mL of ultrapure water (UPW) and stirred for an additional hour at 95 °C. The temperature was rapidly increased, and violent effervescence occurred. Afterward, the temperature was reduced to around 60 °C, and 15 mL of 3% H_2O_2 was added dropwise to reduce the $KMnO_4$. Stirring continued overnight at ambient temperature, during which a yellow tint appeared in the mixture. The suspension was transferred into two 50 mL tubes for easier handling and vigorously mixed using a vortex. The mixture was then centrifuged twice at 6000 rpm for 15 minutes at 25 °C. The resulting black residue was treated with 30 mL of sulfuric acid, 5 mL of hydrogen peroxide, and 965 mL of ultrapure water to remove impurities and oxidant ions. After stirring, the mixture was centrifuged again, and the residue was re-suspended in UPW and dialysed in UPW (cut-off: 14 000 kDa) for 72 hours. Finally, the purified GO (45 mL) was freeze-dried using a Beta 1-8 LSCplus freeze dryer (Christ, Herlev, Denmark), stored in a sealed bottle, and kept in a desiccator until further experiments were conducted.

2.3 GO–Au nanohybrid material synthesis

The GO–Au nanohybrid was synthesised using a modified method based on ref. 21. First, 60 mg of the synthesised GO was dispersed in 750 mL of UPW at room temperature, and the mixture was stirred magnetically for 1 hour. Next, 150 mg of $HAuCl_4$ was added to the GO dispersion, and the solution was stirred continuously for another hour. After that, 75 mL of sodium citrate solution was added, and the mixture was stirred for an additional 30 minutes. The solution was then heated to 80 °C and maintained at this temperature for 1 hour. After cooling, the final dispersion was diluted with UPW and centrifuged three times at 7000 rpm for 15 minutes each time. The supernatant was discarded, and the collected GO–Au nanohybrid was purified using dialysis tubing (molecular weight cut-off: 14 000 kDa) for 48 hours. After purification, the GO–Au nanohybrid (82 mL) was stored in a refrigerator at 4 °C until further use.

2.4 Characterisation and stability studies of the GO–Au nanohybrid

The absorbance of the GO and GO–Au nanohybrid dispersions was measured using UV-vis spectroscopy (UV-2600 Shimadzu spectrophotometer) with quartz cells across a spectral range of 800–200 nm. The zeta potential, indicating

the surface charge of the GO and GO–Au nanohybrid dispersions, was measured using a Malvern Zetasizer (Malvern Instruments Ltd., Worcestershire, UK). The morphology and size distribution of the materials were imaged using transmission electron microscopy (TEM) (JEOL 1400, 80 keV, Hertfordshire, UK) operating at an accelerating voltage of 80 keV. Raman spectra were obtained using a Renishaw InVia system. Atomic force microscopy (AFM) scans were conducted by depositing sample droplets on glass slides and allowing them to dry. The slides were then mounted on the microscope and imaged using peak force tapping on a Multimode 8 microscope with a Nanoscope 5 controller (Bruker, Durham, UK). To analyse the functional groups on GO and GO–Au, Fourier-transform infrared (FTIR) spectroscopy (Perkin Elmer, Beaconsfield, UK) was employed. Additionally, thermogravimetric analysis (TGA) was performed using a Perkin Elmer TGA 8000 system, with a heating rate of 10 °C min^{-1} up to 1000 °C under a synthetic air flow rate of 50 mL min^{-1}.

The dispersion stability of GO and GO–Au nanohybrids (both at a concentration of 100 mg L^{-1}) in DMEM/F12 (supplemented with 10% FBS and 1% penicillin/streptomycin) and UPW was evaluated following a modified version of the OECD 318 guideline (Organisation for Economic Co-operation and Development). The samples remained undisturbed, and 100 μL aliquots were carefully taken from the surface of the dispersion at 0, 24, and 48 hours, ensuring minimal disturbance to the rest of the sample. The stability of the materials was assessed in triplicate by measuring the absorbance of GO at 230 nm using a microplate spectrophotometer (Spark, Tecan, Reading, UK). The surface charge (zeta potential) of the materials was measured using a Zetasizer Nano ZS (model ZEN3600, Malvern Instruments).

2.5 *In vitro* ecotoxicity studies

2.5.1 Cell viability assay. The cell viability of ZF4 cells exposed to GO and GO–Au was assessed using the MTT assay and mLDH according to methods described.[22,23] The cells were seeded into transparent 96-well flat-bottom plates at a density of 10 000 cells per well in 100 μL of DMEM/F12 (supplemented with 10% FBS and 1% penicillin/streptomycin) and incubated overnight. After 24 hours, the cells were treated with varying concentrations of GO and GO–Au (ranging from 2.5 to 150 mg L^{-1}) for 24, 48, and 72 hours. Positive control cells were treated with 20% dimethyl sulfoxide (DMSO), while negative control cells were treated with DMEM/F12 (supplemented with 10% FBS and 1% penicillin/streptomycin) only. A stock solution of MTT (5 mg mL^{-1}) was prepared in sterile phosphate-buffered saline (PBS) and filtered through a 0.2 μm Acrodisc syringe filter. After the treatment period, the medium was removed, and 120 μL of the MTT solution, diluted in DMEM/F12 (supplemented with 10% FBS and 1% penicillin/streptomycin) at a 1 : 6 ratio, was added to each well. After 4 hours of incubation, the MTT solution was replaced with 200 μL of DMSO to solubilise the formazan crystals. This was done in the dark with gentle agitation for 15 minutes. The absorbance of each well was then measured at 570 nm using a microplate reader. For the mLDH, the cells were lysed according to the manufacturer's instruction and the absorbance was measured at 490 nm.

2.5.2 Flow cytometry measurement of ROS. A CellROX Deep Red reagent kit (Paisley, UK) was used to determine ROS generation in ZF4 cells as described by ref. 24. Briefly, ZF4 cells were seeded into 6-well plates at a density of 2×10^5 cells per well and incubated overnight. The following day, the cells were treated with GO and GO–Au at concentrations of 1, 50, and 100 μg mL^{-1} for 24 hours, while a positive control was treated with 50 μM menadione for 1 hour. After incubation, the cells were detached using trypsin and centrifuged at 1500 rpm for 5 minutes. The cell pellets were then stained with 5 μM CellROX Deep Red reagent, diluted in phenol-free RPMI 1640 medium, and incubated at 37 °C in the dark for 1 hour. ROS production was analysed using a BD LSRFortessa X20 cell analyser by acquiring data from 10 000 events.

2.5.3 Apoptosis and necrosis assay. The induction of apoptosis and necrosis in ZF4 cells exposed to GO and GO–Au was assessed using an Alexa Fluor 488 annexin V/PI assay kit, following the manufacturer's protocol. Briefly, ZF4 cells were seeded into 6-well plates at a density of 2×10^5 cells per well and incubated overnight. The next day, the cells were treated with GO and GO–Au at concentrations of 1, 50, and 100 μg mL^{-1} for 24 hours. Positive control cells were treated with 10% DMSO for 24 hours and 1 μM staurosporine for 6 hours to induce necrosis and apoptosis, respectively. After treatment, the cells were detached using trypsin and centrifuged at 1500 rpm for 5 minutes at 4 °C. The resulting cell pellet was resuspended in 100 μL of annexin binding buffer, followed by incubation with 1 μL of propidium iodide (PI) and 5 μL of annexin V-FITC for 15 minutes in the dark at room temperature. Following incubation, the cell suspension was diluted with 400 μL of annexin binding buffer and analysed using the BD LSRFortessa X20 cell analyser, acquiring data from 10 000 events. Spectral overlap between the fluorophores was electronically compensated during the analysis.

2.6 Statistical analysis

All data are presented as the mean ± standard deviation (SD) of triplicate independent experiments and analysed using GraphPad prism software version 9.0 (GraphPad Inc., USA). One-way analysis of variance (ANOVA) followed by Bonferroni's *post hoc* test for multiple comparisons was used to calculate the differences between groups. $P < 0.05$ indicates statistically significant difference.

3. Results and discussion

3.1 Physicochemical characterisation and stability studies

Understanding the dispersion stability and physicochemical properties of NMs like GO and GO–Au nanohybrids is critical for predicting their biological interactions and overall

toxicity. The stability of GO and GO–Au in DMEM/F12 influences their uptake by cells, interactions with biomolecules, and potential toxicological effects.[25] In this study, we assessed the dispersion stability of GO and GO–Au nanohybrids in both UPW and DMEM/F12 (supplemented with 10% FBS and 1% penicillin/streptomycin) to simulate their behaviour in biological environments.

Complementary to the dispersion stability, the TEM analysis of GO and GO–Au nanohybrids provides insights into their morphological characteristics. Fig. 1A shows that GO exhibited a layered and wrinkled morphology typical of two-dimensional materials. The AFM images (Fig. S1†) agree with TEM data confirming the size and morphology of GO. Fig. 1B and C illustrate the deposition of Au nanoparticles on GO, and Fig. 1C provides a magnified view of the same, highlighting the distribution of Au nanoparticles on the GO sheets. The magnified TEM images of the GO–Au nanohybrids confirm the successful decoration of AuNPs on the surface of GO sheets. The uniform distribution of AuNPs enhances the surface area of the hybrid material, which could improve its reactivity and interaction with biological molecules, as well as its colloidal stability.

FTIR spectroscopy further supports the successful synthesis of GO–Au nanohybrids by highlighting changes in the surface chemistry of the materials. The FTIR spectrum of GO (Fig. 1D) shows characteristic peaks at ~1730 cm^{-1} corresponding to C=O stretching of carboxyl groups and ~1220 cm^{-1} for C–O stretching of epoxy groups. In the case of GO–Au, the intensity of the C=O (1700 cm^{-1}) is significantly diminished, along with a decrease in the percentage of transmittance, suggesting that GO undergoes reduction during the synthesis of GO–Au nanohybrids. This reduction in peak intensity indicates that the AuNPs likely bind to these functional groups, altering the surface chemistry of GO, which can influence its biological interactions and reduce its cytotoxicity. These chemical modifications likely contribute to the observed stability improvements and reduced toxicological impact of GO–Au nanohybrids compared to GO.

TGA was used to assess the thermal stability of GO and GO–Au nanohybrids. As observed in Fig. 1E, GO exhibits a significant weight loss between 200 °C and 300 °C due to the decomposition of oxygen-containing functional groups. In contrast, GO–Au nanohybrids display a more gradual weight loss, with higher thermal stability compared to GO. The presence of AuNPs on the GO surface appears to delay the decomposition of the material, providing enhanced thermal stability.

The Raman spectra of GO and GO–Au nanohybrids (Fig. 1F) display the characteristic D (~1350 cm^{-1}) and G

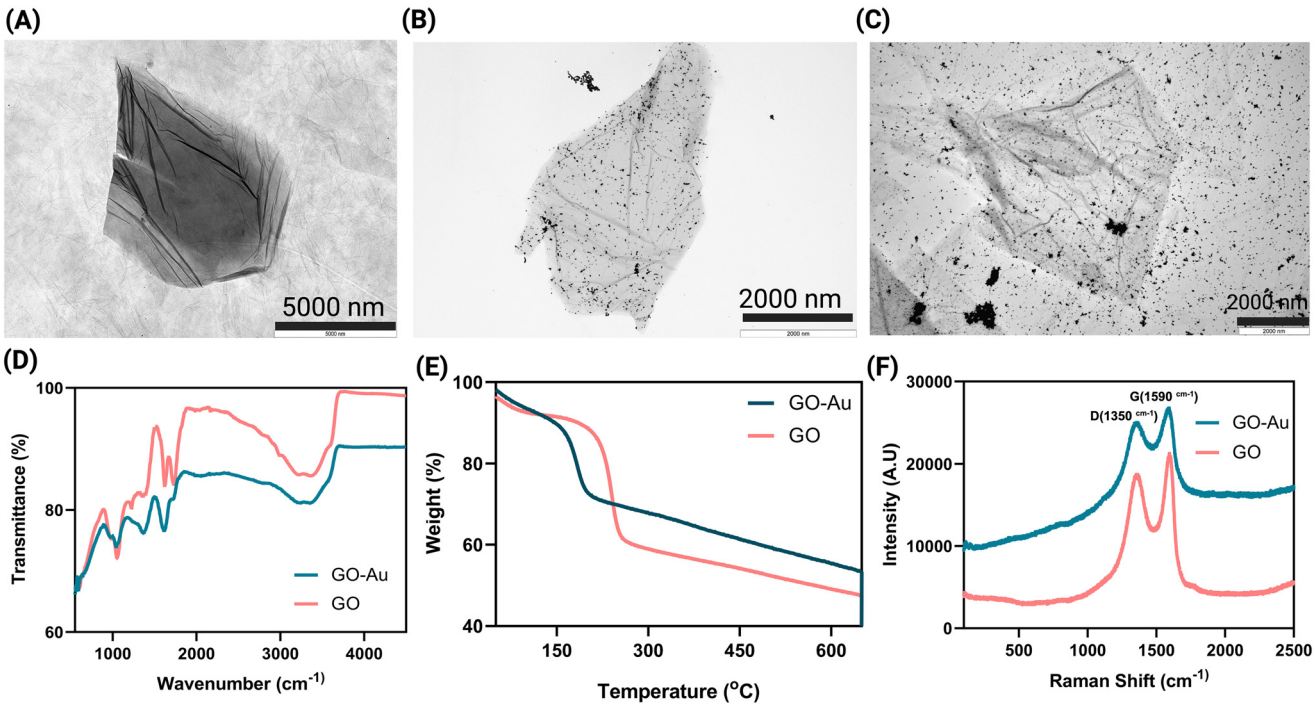

Fig. 1 Physicochemical characterization and stability of GO and GO–Au nanohybrids. (A) Transmission electron microscopy (TEM) image of GO showing its layered structure with a wrinkled morphology. (B) and (C) TEM images of the GO–Au nanohybrid, demonstrating the uniform distribution of AuNPs on the GO sheets. (D) Fourier-transform infrared (FTIR) spectra of GO and GO–Au nanohybrids. For GO, characteristic peaks include the C=O stretching at ~1730 cm^{-1} and C–O stretching at ~1220 cm^{-1}. For GO–Au, the C=O peak is less intense, indicating interaction between AuNPs and oxygen-containing groups on GO. (E) TGA curves showing weight loss profiles of GO and GO–Au. GO exhibits a weight loss at around 200–300 °C due to decomposition of oxygen-containing functional groups, while GO–Au displays a more gradual weight loss, indicating enhanced thermal stability. (F) Raman spectra of GO and GO–Au nanohybrids, highlighting the D (~1350 cm^{-1}) and G (~1590 cm^{-1}) bands. The D/G intensity ratio is higher for GO–Au, indicating structural changes due to AuNP decoration.

(~1590 cm^{-1}) bands, which correspond to the disorder and graphitic sp^2 carbon domains, respectively. The D/G intensity ratio is higher for GO–Au than for GO, indicating that the attachment of AuNPs increases structural disorder in the GO sheets. This increased disorder may affect the electronic properties of GO–Au nanohybrids, influencing their interactions with cells and biomolecules. However, this increases in disorder, combined with the modified surface chemistry, may also contribute to the enhanced stability and reduced toxicity of GO–Au nanohybrids compared to GO. XPS was conducted to determine the elemental composition of GO and GO–Au nanohybrids. The analysis revealed that the composition of GO includes 31.85% oxygen and 68.15% carbon, consistent with its structure and expected oxygen-containing functional groups. For the GO–Au nanohybrids, the elemental composition was found to be 29.83% oxygen, 67.15% carbon, and 3.02% gold, as shown in Tables S1 and S2 in the ESI.† The presence of gold in the nanohybrids confirms successful integration of gold nanoparticles into the GO matrix. Furthermore, the slight reduction in oxygen content in the hybrids compared to pure GO suggests a partial reduction of oxygen-containing functional groups during the synthesis process, likely due to the interaction with gold precursors or the reduction process involved in hybrid formation. Additionally, we analysed the concentration of manganese (Mn) (a known impurity in GO

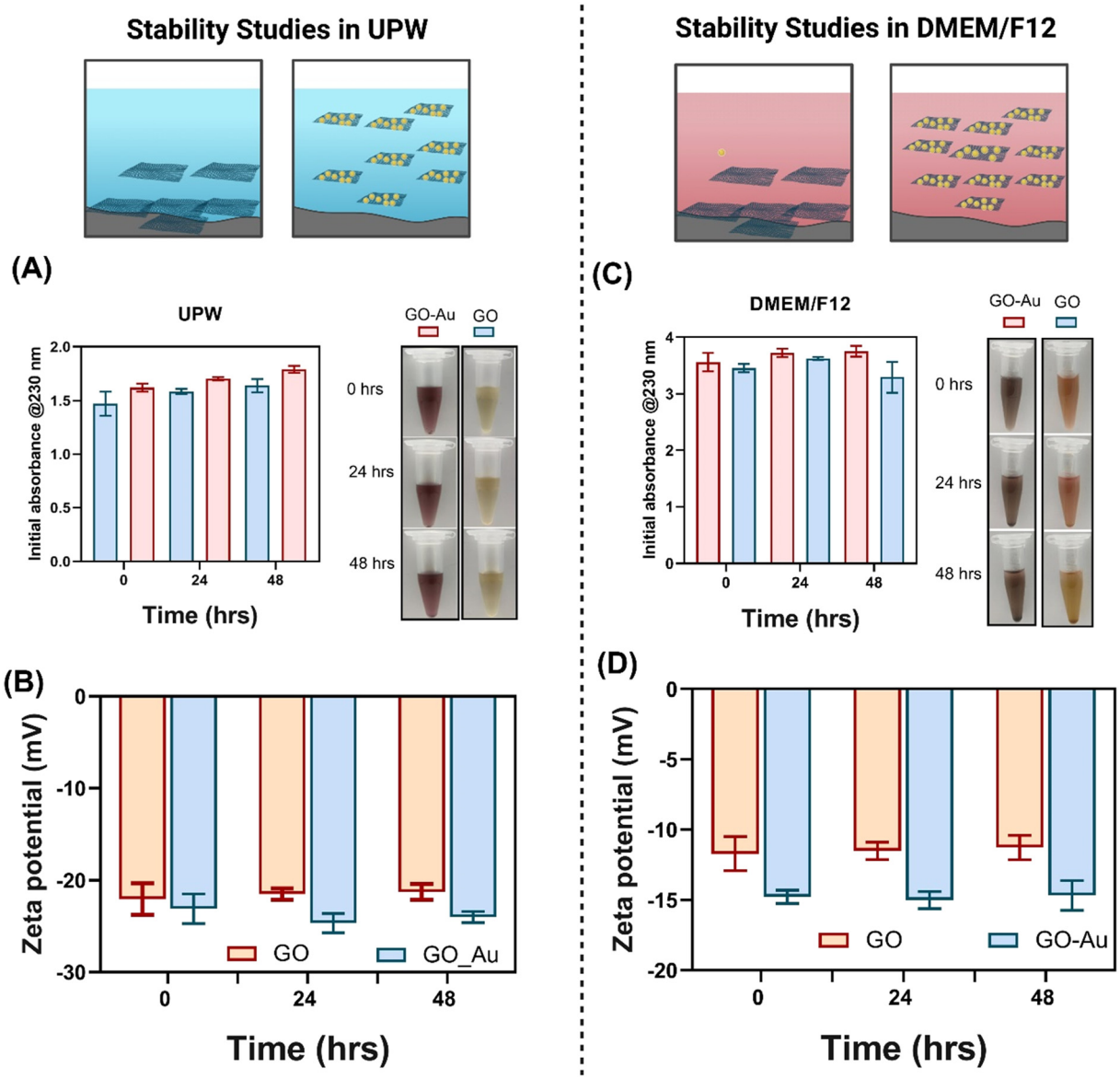

Fig. 2 Stability studies of GO and GO–Au nanohybrids in ultrapure water (UPW) and DMEM/F12 over 48 hours. (A) and (C) show average absorbance measurements at 230 nm, with GO–Au maintaining superior dispersion stability compared to GO in both UPW and DMEM/F12 (supplemented with 10% FBS and 1% penicillin/streptomycin). (B) and (D) represent the zeta potential measurements, demonstrating that GO–Au nanohybrids exhibit more negative zeta potential values than GO, indicating better colloidal stability. The inset images show visual comparisons of sedimentation over 0, 24, and 48 hours for each material in both UPW and DMEM/F12, with GO visibly aggregating more rapidly than GO–Au.

synthesis due to the use of $KMnO_4$ in Hummer's method) in the GO–Au nanohybrids using acid digestion followed by ICP-MS. The results revealed a negligible Mn content of 2.031 ± 0.16 ppb, indicating minimal contamination or a residual precursor material in the hybrid.

The UV-vis absorbance at 230 nm, a characteristic peak for GO, was utilised to assess the dispersion stability of the materials. Fig. 2(A and C) illustrate that both GO and GO–Au exhibited excellent stability over time in UPW and DMEM/F12 (supplemented with 10% FBS and 1% penicillin/streptomycin). In UPW, GO and GO–Au retained nearly all their initial absorbance after 24 and 48 hours, demonstrating negligible sedimentation (Fig. 2A). Similarly, in DMEM/F12, both materials maintained a high proportion of their initial absorbance over 48 hours, with GO–Au showing slightly improved stability compared to GO alone (Fig. 2C). This improvement can be attributed to interactions between AuNPs and biomolecules in DMEM/F12, which likely reduce aggregation and enhance colloidal stability.[26] Despite minor sedimentation over time, the overall dispersion remained robust. The characteristic UV-vis peaks of AuNPs and GO at 520 nm and 230 nm, respectively, confirm the successful formation of GO–Au nanohybrids (Fig. S2†). The remarkable stability of GO–Au nanohybrids in DMEM/F12 is particularly significant, as dispersion stability is a critical factor influencing the bioavailability and toxicity of materials. Prior research has demonstrated that unstable NMs often form aggregates, reducing cellular uptake and potentially altering their toxicological behaviour.[27,28] In our study, the observed subtle increases in absorbance for GO–Au nanohybrids over time, approximately a marginal rise (0.163 nm) after 24 hours and a slightly higher increase after 48 hours (0.196 nm), suggest that AuNPs contribute to enhanced colloidal stability.[29] In addition, both GO and GO–Au shows a negatively charged zeta potential in UPW (Fig. 2B) and DMEM/F12 (Fig. 2C), with GO–Au being more negatively charged compared to GO alone, indicating its enhanced stability in both water and DMEM/F12.

3.2 Reduced cytotoxicity and oxidative stress in ZF4 cells treated with GO–Au nanohybrids compared to GO

The cytotoxic effects of GO and GO–Au nanohybrids on ZF4 cells were evaluated using both cell viability (*via* mLDH) and metabolic activity (MTT assay) as indicators. These assessments revealed a clear relationship between increasing concentrations of GO and GO–Au (2.5 to 150 μg mL^{-1}) and the duration of exposure (24 to 72 hours) with decreasing cell viability and metabolic activity, as shown in Fig. 3.

After 24 hours of incubation, the viability of ZF4 cells exposed to GO was preserved at concentrations up to 10 μg mL^{-1} but began to decrease significantly from 20 μg mL^{-1} onwards (Fig. 3A). The most substantial reduction in cell viability was observed at 150 μg mL^{-1}, with 41.7% viability after 48 hours and 39.5% after 72 hours. A similar dose- and time-dependent trend was seen in the metabolic activity of GO-treated cells (Fig. 3C). After 24 hours, the metabolic activity was maintained up to 10 μg mL^{-1} but started to decrease from 20 μg mL^{-1}, with the most significant reduction observed at 150 μg mL^{-1} after 72 hours (a drop to 29.8%).

ZF4 cells exposed to GO–Au nanohybrids exhibited similar trends in cytotoxicity, but with slightly reduced severity. As shown in Fig. 3B, all GO–Au treatments led to a significant decrease in cell viability after 24 hours, except for the lowest concentrations (2.5 and 5 μg mL^{-1}). After 48 and 72 hours, cells exposed to concentrations above 5 μg mL^{-1} showed a marked reduction in viability, with the highest concentration (150 μg mL^{-1}) leading to a decrease to 54.5% after 72 hours. Similarly, GO–Au-treated cells exhibited a dose- and time-dependent reduction in metabolic activity, starting at 40 μg mL^{-1} after 24 hours and at 5 μg mL^{-1} after 48 and 72 hours (Fig. 3D).

To understand the cytotoxic response of ZF4 cells based on the mass fraction of GO and Au, we conducted elemental analysis of the GO–Au nanohybrids *via* sample digestion in *aqua regia*, followed by ICP-MS measurements to determine the concentration and mass fraction of Au in the hybrids. The analysis revealed that in 150 μg mL^{-1} GO–Au nanohybrids, the Au concentration is 52.23 ± 1.99 μg mL^{-1}, while the GO concentration is 97.73 ± 1.99 μg mL^{-1}. These results, now included in the ESI† (Fig. S3), confirm that GO remains the dominant component of the hybrid material and validate the intended composition. We replotted the cytotoxicity data based on the equivalent GO mass concentration. Specifically, we compared the effect of 100 μg mL^{-1} standalone GO to that of the 97.73 μg mL^{-1} GO content in 150 μg mL^{-1} GO–Au nanohybrids. The results demonstrated that after 24 hours, standalone GO reduced the metabolic activity of ZF4 cells to 62.69%, whereas GO–Au nanohybrids increased the metabolic activity by approximately 6% (Fig. S4†). Furthermore, after 48 hours, the metabolic activity of the cells increased to ~10% by 50 μg mL^{-1} GO–Au nanohybrids compared to 100 μg mL^{-1} standalone GO. Importantly, this result was observed even without accounting for the cytotoxic contribution of the Au component (52.23 ± 1.99 μg mL^{-1}). To further investigate the effect of gold nanoparticles, we conducted additional cytotoxicity assays at the equivalent Au concentration (52 μg mL^{-1}) as found in the GO–Au nanohybrids. The results showed negligible effects of Au nanoparticles on metabolic activity (Fig. S5†). This finding reinforces the conclusion that the attachment of gold nanoparticles to GO mitigates its aggregation and sedimentation, thereby reducing its interaction with cells and overall cytotoxicity.

The results clearly demonstrate that both GO and GO–Au nanohybrids induce dose-dependent cytotoxicity in ZF4 cells. However, GO–Au nanohybrids exhibited a relatively less toxic profile, particularly at higher concentrations. The reduction in cytotoxicity observed upon binding AuNPs to C═O functional groups on GO can be attributed to several interconnected mechanisms. First, the binding of AuNPs

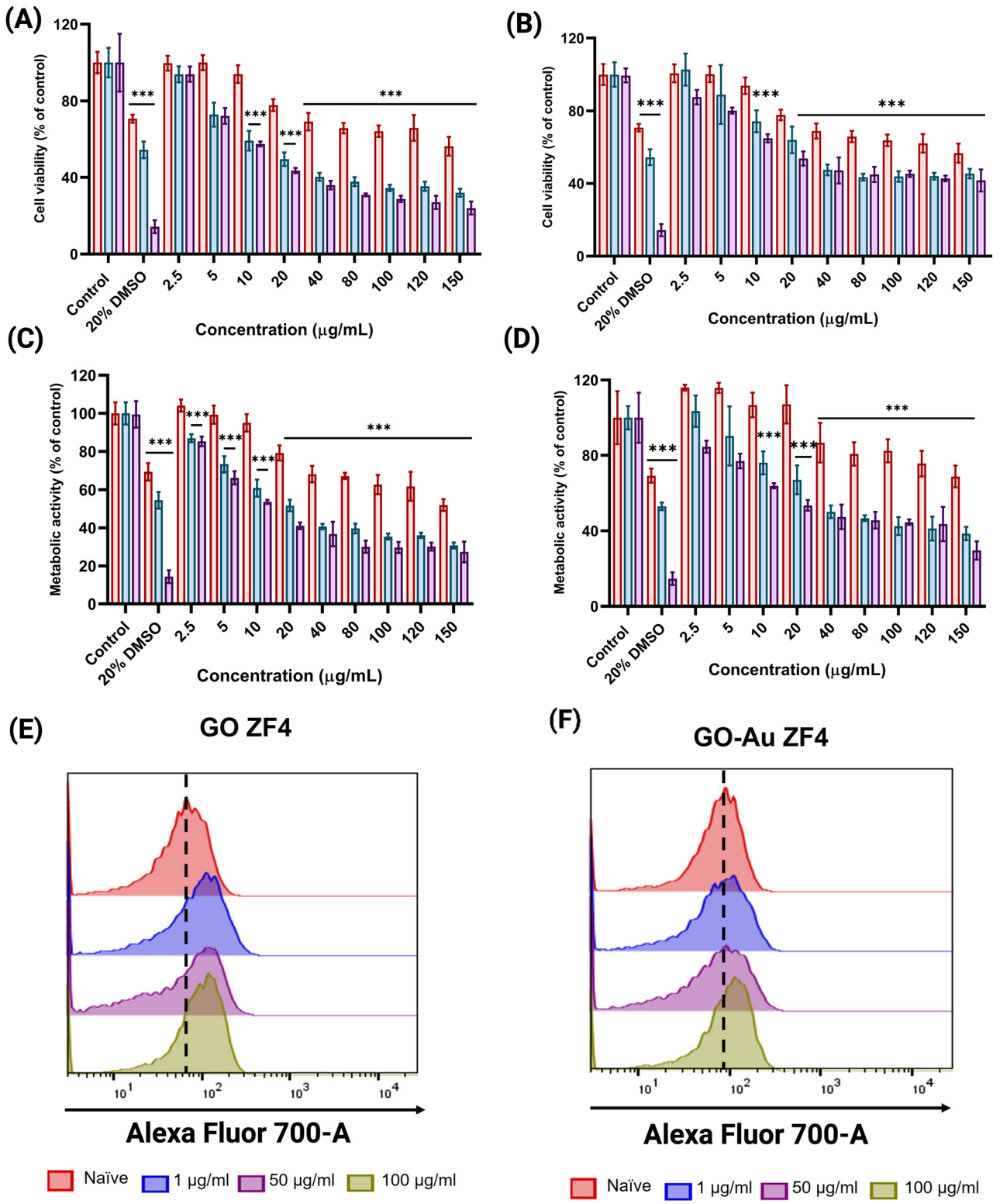

Fig. 3 Cytotoxicity and metabolic activity of ZF4 cells exposed to GO and GO–Au nanohybrids. (A) Cell viability of ZF4 cells treated with GO for 24, 48, and 72 hours, as measured by the modified LDH assay, across a concentration range of 2.5 to 150 μg mL^{-1}; (B) cell viability of ZF4 cells treated with GO–Au nanohybrids, measured by the mLDH assay across the same concentration range and time periods; (C) metabolic activity of ZF4 cells treated with GO measured by the MTT assay across the same concentration range and time periods; (D) metabolic activity of ZF4 cells treated with GO–Au, assessed using the MTT assay across the concentration range of 2.5 to 150 μg mL^{-1}; (E and F) flow cytometry analysis for ROS production in ZF4 cells exposed to GO (E) and GO–Au nanohybrids (F) at concentrations of 1, 50, and 100 μg mL^{-1} for 24 hours. The dashed vertical line indicates the mean intensity of the control cells for comparison. 20% DMSO was used as a positive control, and data are expressed as the mean ± standard deviation from triplicate independent experiments. Asterisks indicate statistically significant differences compared to naïve (untreated) cells: ***$p < 0.001$.

reduces the availability of reactive oxygen-containing groups on the GO surface, subsequently decreasing the generation of ROS, a primary driver of cytotoxicity. FTIR results support this, showing a reduced intensity of the C=O peak, which indicates altered surface chemistry of GO. These changes moderate its interactions with cellular membranes and biomolecules, mitigating oxidative stress pathways that typically lead to cell death. Furthermore, this interaction enhances the colloidal stability of GO–Au hybrids in biological media, as demonstrated by zeta potential measurements and sedimentation analyses. Enhanced stability prevents the formation of large aggregates, which are known to exacerbate cellular stress and have cytotoxic effects.[30] These factors collectively contribute to the observed reductions in necrosis and apoptosis rates in ZF4 cells treated with GO–Au nanohybrids compared to GO alone.

In support of these findings, studies such as ref. 31 have demonstrated that surface modifications can improve stability and circulation of nanoparticles by protecting them from immune recognition and clearance, further supporting the reduced cytotoxicity observed in our study. Additionally, Gonzalez-Garcia *et al.*[32] reported that nanoparticles enriched with carboxylic acid functionalities enhance pro-inflammatory cytokine production due to increased complement protein levels. In contrast, our study highlights that the incorporation of AuNPs into GO alters its surface chemistry in a manner that mitigates inflammatory and oxidative stress responses. This suggests that, unlike carboxylic acid-enriched nanoparticles that amplify inflammatory effects, the interaction of AuNPs with oxygen-containing functional groups on GO stabilises the material and reduces ROS generation, leading to improved safety profiles. These findings reinforce the broader concept that tailoring surface chemistry of nanoparticles can direct physiological responses, thereby enhancing their safety and biocompatibility.

This attenuation in cytotoxicity is likely due to the presence of gold nanoparticles, which enhance the colloidal stability of the nanohybrids, reducing aggregation and sedimentation. These findings align with previous studies suggesting that stability of NMs plays a crucial role in influencing their bioavailability and cellular uptake.[33,34]

This study represents the first known investigation into the cytotoxic effects of GO and GO–Au nanohybrids on ZF4 cells, filling a critical gap in the existing literature. Previous studies have reported the cytotoxicity of other NMs to ZF4 cells, such as silver nanoparticles[35,36] and lanthanides,[37] but no comprehensive evaluation of GO or GO–Au nanohybrids has been conducted in this specific cell line. The observed cytotoxicity to ZF4 cells is consistent with other NMs, but the comparative reduction in toxicity seen with GO–Au nanohybrids highlights their potential for safer applications due to enhanced dispersion and reduced aggregation.

The bioavailability and dispersion stability of NMs are key factors influencing their cytotoxicity. GO, due to its propensity to agglomerate and form sediments, can exhibit higher toxicity as larger aggregates are more likely to interact with and damage cellular structures.[38] In contrast, the enhanced stability of GO–Au nanohybrids in DMEM/F12 likely plays a protective role by minimising aggregation, thereby reducing cellular interactions that lead to cytotoxicity. This finding is supported by the fact that even at high concentrations, GO–Au nanohybrids induced less severe cytotoxic effects compared to GO alone.

The stability of GO and GO–Au nanohybrids in DMEM/F12, as demonstrated in this study, may have significantly contributed to the cytotoxic effects observed in the treated cells. NMs that maintain stable dispersions in biological media are more likely to interact with cells uniformly, leading to more predictable and potentially less harmful biological responses.[9] These findings highlight the importance of evaluating the stability of NMs when assessing their potential risks in biological and environmental applications.

ROS are naturally produced in cells as by-products of normal cellular metabolism, playing key roles in cell signalling and homeostasis.[39] However, excessive ROS production, often triggered by environmental stressors or foreign substances like nanoparticles, can lead to oxidative stress, damaging cellular structures, including lipids, proteins, and DNA.[40] This oxidative stress is a precursor to various diseases and cellular dysfunction.

In our study, ROS generation was evaluated in ZF4 cells treated with different concentrations (1, 50, and 100 μg mL^{-1}) of GO and GO–Au nanohybrids using the CellROX Deep Red assay. Fig. 3E and F clearly illustrate a dose-dependent increase in ROS production in ZF4 cells for both GO and GO–Au treatments, confirming that the exposure to these NMs leads to oxidative stress. Interestingly, while both materials induced significant ROS production, the levels generated by GO alone were consistently higher than those observed in cells treated with GO–Au nanohybrids. As shown in Fig. 3E, at concentrations of 50 and 100 μg mL^{-1}, GO elicited a substantial spike in ROS generation, with much stronger intensity compared to GO–Au nanohybrids (Fig. 3F). This suggests that the incorporation of AuNPs into the GO matrix reduces the oxidative stress typically associated with GO exposure, likely due to the enhanced stability and reduced agglomeration of the GO–Au nanohybrids.

The relationship between ROS production and nanoparticle characteristics, such as concentration, surface functionalisation, and lateral size, has been well-documented.[41] Larger GO aggregates and unstable dispersions tend to interact more intensively with cellular components, leading to increased ROS production and, consequently, more severe oxidative stress. In contrast, the improved dispersion stability of GO–Au nanohybrids likely limits their interaction with cellular membranes and intracellular components, resulting in reduced ROS generation. These findings highlight the importance of nanoparticle surface modification in mitigating the cytotoxic effects associated with ROS overproduction. By reducing ROS levels, GO–Au nanohybrids demonstrate enhanced

biocompatibility compared to GO, making them more suitable for applications where minimising oxidative damage is critical. The dose-dependent nature of the ROS response in this study reinforces the need to carefully control nanoparticle concentrations to avoid oxidative stress-related cytotoxicity in biological systems.

3.3 Gold nanoparticles in GO–Au nanohybrids mitigate apoptosis and necrosis in ZF4 cells

Cell death, through mechanisms such as apoptosis and necrosis, plays a critical role in maintaining cellular homeostasis.[24] In this study, both apoptosis (regulated cell death) and necrosis (pathological cell death) were evaluated in ZF4 cells exposed to GO and GO–Au nanohybrids. As seen in Fig. 4, there is a clear dose-dependent increase in both apoptotic and necrotic cell populations with increasing concentrations of GO and GO–Au (1, 50, and 100 μg mL^{-1}).

Fig. 4A shows flow cytometry scatter plots illustrating the apoptotic and necrotic responses of ZF4 cells following treatment with GO and GO–Au nanohybrids at concentrations of 1, 50, and 100 μg mL^{-1}. These scatter plots visually differentiate between live cells, early apoptotic cells, late apoptotic cells, and necrotic cells based on staining with annexin V and propidium iodide (PI). In the control and DMSO groups, most cells are in the bottom left quadrant (Q3), which represents live cells that are negative for both annexin V and PI. In contrast, with increasing concentrations of GO and GO–Au, there is a notable shift in cell populations towards the other quadrants, particularly Q2 (late apoptotic cells, annexin V^+/PI^+) and Q1 (necrotic cells, annexin V^-/PI^+). For cells treated with 100 μg mL^{-1} GO, a large number of cells appear in Q1, indicating high levels of necrosis, while cells treated with GO–Au at the same concentration show fewer necrotic cells and more live cells in Q3. This difference supports the conclusion that GO–Au nanohybrids induce less severe cell death compared to GO, likely due to the mitigating effects of AuNPs on oxidative stress and cellular interactions. Fig. 4A visually demonstrates the dose-dependent increase in apoptosis and necrosis in ZF4 cells exposed to both GO and GO–Au, with GO inducing more severe cellular damage compared to GO–Au, especially at

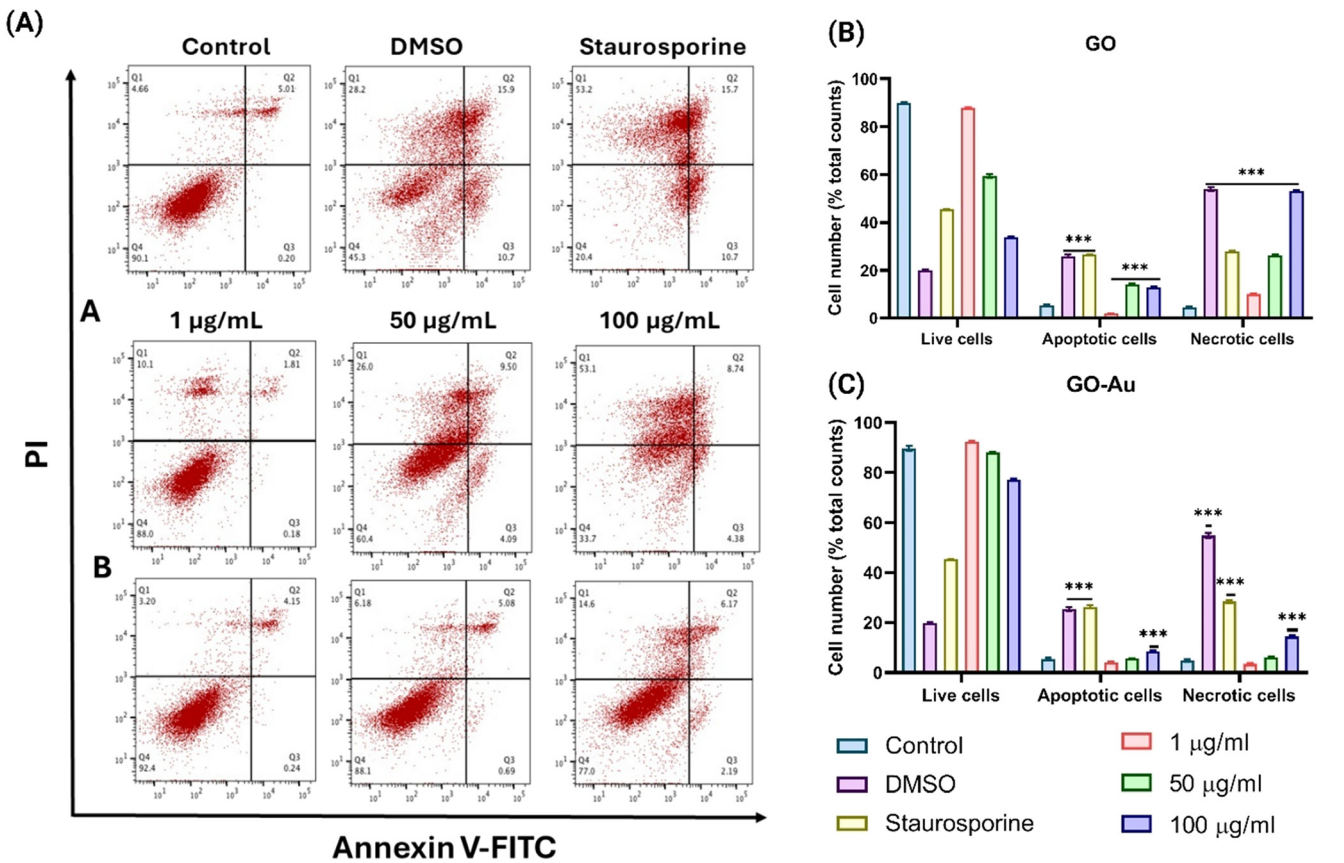

Fig. 4 Apoptosis and necrosis of ZF4 cells exposed to GO and GO–Au nanohybrids. (A) Flow cytometry scatter plots of ZF4 cells treated with GO (A) and GO–Au (B) nanohybrids at 1, 50, and 100 μg mL^{-1} for 24 hours, stained with annexin V and propidium iodide (PI) to differentiate live, apoptotic, and necrotic cells. Controls include untreated cells (control), DMSO (apoptosis control), and staurosporine (apoptosis/necrosis control). (B) Quantification of cell populations treated with GO, showing a dose-dependent increase in apoptosis and necrosis, particularly at 50 and 100 μg mL^{-1} ($p < 0.001$). (C) Quantification of cell populations treated with GO–Au, showing reduced cytotoxicity compared to GO, with fewer apoptotic and necrotic cells at higher doses ($p < 0.001$). Both treatments show dose-dependent effects but GO–Au nanohybrids exhibit less cytotoxicity. Data are presented as the mean ± SD, with significant differences ($p < 0.001$) indicated by ***.

higher concentrations. This further supports the hypothesis that the incorporation of AuNPs into GO helps reduce cytotoxic effects by enhancing colloidal stability and limiting cellular damage.

GO induced higher levels of apoptosis and necrosis compared to GO–Au, suggesting that the AuNP component mitigates some of the cytotoxic effects typically associated with GO exposure. Specifically, at the highest concentration (100 μg mL^{-1}), GO–Au nanohybrids induced 14.6% necrosis, while GO alone induced a significantly higher level of necrosis at 53.1% (Fig. 4B and C). This disparity highlights the role of AuNPs in reducing GO-induced cellular damage, possibly due to improved colloidal stability and decreased agglomeration, which limit the interactions of the NMs with cell membranes.

The ability of GO and related materials to induce apoptosis and necrosis has been widely documented.[42] The physicochemical characteristics of GO—such as surface chemistry, lateral dimensions, and the presence of oxygen-containing functional groups—are thought to activate several signalling pathways that promote apoptosis.[43] Previous studies have shown that exposure to high concentrations of GO can lead to excessive ROS production, which damages mitochondria and accelerates apoptosis.[44,45]

The lower apoptosis and necrosis rates observed with GO–Au nanohybrids are likely a result of their enhanced stability, which reduces the overproduction of ROS and subsequent oxidative stress (as previously shown in Fig. 3E and F). The integration of AuNPs within the GO matrix appears to prevent the excessive aggregation typical of GO alone, thereby limiting cellular uptake and mitigating cytotoxic effects. This difference in apoptosis and necrosis between GO and GO–Au can be directly correlated with the overall physicochemical characteristics of the NMs. GO's tendency to form aggregates leads to increased cellular interactions and ROS generation, triggering higher rates of apoptosis and necrosis. In contrast, the enhanced dispersion of GO–Au nanohybrids helps limit these detrimental interactions, resulting in a less pronounced cytotoxic response. The high necrosis rates observed with GO, particularly at elevated concentrations, suggest potential pathological consequences if these materials are released into the environment. Prolonged exposure to GO could result in cellular damage, compromising the health of aquatic organisms that are integral to the food chain. On the other hand, the reduced cytotoxicity and ROS generation observed with GO–Au nanohybrids indicate their potential as a safer alternative in biological and environmental applications.

4. Conclusions and outlook

This study provides essential insights into the cytotoxicity and oxidative stress effects of GO and GO–Au nanohybrids, underscoring the importance of the safe and sustainable by design framework in material development. By addressing the limitations of GO, particularly its cytotoxicity and tendency to aggregate, the integration of AuNPs demonstrates a promising pathway towards safer and more sustainable NMs.

The results reveal that GO–Au nanohybrids exhibit significantly reduced cytotoxicity compared to pristine GO. This reduction can be attributed to the stabilising effect of AuNPs, which improve colloidal stability and reduce the availability of reactive oxygen-containing functional groups responsible for generating ROS. The mitigated oxidative stress and decreased levels of apoptosis observed in ZF4 cells highlight the enhanced biocompatibility of GO–Au nanohybrids. These findings not only contribute to a better understanding of GO's toxicological profile but also provide a clear strategy for modifying NMs to improve safety without compromising their functional properties.

From an environmental perspective, the enhanced colloidal stability of GO–Au nanohybrids reduces their propensity to aggregate and sediment, thereby minimising the risk of unintended accumulation in aquatic ecosystems. This improved stability aligns with SSbD principles, which emphasise the need to reduce environmental impacts across the material lifecycle, from synthesis to disposal. By demonstrating reduced toxicity and improved environmental behaviour, GO–Au nanohybrids exemplify how advanced materials can be engineered for sustainability and safety in various applications, including biosensing, drug delivery, and environmental remediation.

Importantly, this study highlights the utility of ZF4 cells as a reliable and high-throughput *in vitro* model for assessing the toxicity of NMs. The use of ZF4 cells aligns with the 3R principles (replacement, reduction, and refinement), promoting sustainable alternatives to traditional animal testing. This approach not only reduces ethical concerns but also enables the generation of robust baseline data on NMs dispersion and biological effects, further supporting SSbD implementation.

Looking forward, a deeper understanding of the long-term biological and environmental impacts of GO–Au nanohybrids is critical for their safe deployment. Future studies should investigate their environmental fate, bioaccumulation potential, and interactions with diverse biological systems across ecosystems. This will provide a comprehensive assessment of their lifecycle impacts, ensuring alignment with sustainability goals. Additionally, further optimisation of the safe by design approach could involve the incorporation of other biocompatible elements or surface coatings. Exploring materials such as polymers, biomolecules, or green-synthesised nanoparticles could further enhance the safety and functionality of GO-based hybrids, expanding their applicability in biomedical, environmental, and industrial settings.

Our study establishes GO–Au nanohybrids as a model for integrating SSbD principles into NMs design. By

demonstrating how strategic modifications can improve the safety profile of GO while preserving its beneficial properties, this work sets the foundation for advancing safer and more sustainable nanotechnology. The insights generated here not only address critical challenges related to nanomaterial toxicity but also pave the way for the responsible innovation and deployment of advanced materials in real-world applications.

Data availability

The data supporting this article have been included as part of the ESI.†

Author contributions

B. I. – conceptualisation, experimentation, original draft, visualisation, writing – review & editing; THA – conceptualisation, experimentation, original draft, visualisation; PD – visualisation, writing – review & editing; E. V. J. writing – review & editing, funding acquisition; S. C. – conceptualisation, supervision, original draft, visualisation, writing – review & editing, funding acquisition.

Conflicts of interest

There are no conflicts to declare.

Acknowledgements

BI and EV-J acknowledge the European Union's Horizon Europe Research & Innovation Programme under grant agreement no. 101092796 (ACCORDs – Green deal inspired correlative imaging-based characterization for safety profiling of 2D materials). SC acknowledges the UKRI NERC Independent Research Fellowship (Grant number – UKRI187), the Engineering and Physical Sciences Research Council Co-Fund [grant number EP/X525662/1], and The Royal Society International Exchange award (IES\R1\241020).

References

1 N. S. Ekal, R. Patil, N. Ranjan, P. Bahadur and S. Tiwari, Oxidation state of graphene oxide nanosheets drives their interaction with proteins: A case of bovine serum albumin, *Colloids Surf., B*, 2022, **212**, 112367.
2 A. M. Z. de Medeiros, L. U. Khan, G. H. da Silva, C. A. Ospina, O. L. Alves and V. L. de Castro, *et al.*, Graphene oxide-silver nanoparticle hybrid material: an integrated nanosafety study in zebrafish embryos, *Ecotoxicol. Environ. Saf.*, 2021, **209**, 111776.
3 T. Ye, Y. Yang, J. Bai, F. Y. Wu, L. Zhang and L. Y. Meng, *et al.*, The mechanical, optical, and thermal properties of graphene influencing its pre-clinical use in treating neurological diseases, *Front. Neurosci.*, 2023, **17**, 1162493.
4 T. H. Akere, A. M. Z. de Medeiros, D. S. T. Martinez, B. Ibrahim, H. Ali-Boucetta and E. Valsami-Jones, Synthesis and Characterisation of a Graphene Oxide-Gold Nanohybrid for Use as Test Material, *Nanomaterials*, 2022, **13**(1), 31.
5 T. H. Akere, A. M. Zigiotto de Medeiros, D. S. T. Martinez, B. Ibrahim, H. Ali-Boucetta and E. Valsami-Jones, Nanotoxicity of Graphene Oxide - Gold Nanohybrid to Daphnia magna, *Aquat. Toxicol.*, 2023, **260**, 106552.
6 T. Fan, L. Yan, S. He, Q. Hong, F. Ai and S. He, *et al.*, Biodistribution, degradability and clearance of 2D materials for their biomedical applications, *Chem. Soc. Rev.*, 2022, **51**(18), 7732–7751.
7 G. Peng and B. Fadeel, Understanding the bidirectional interactions between two-dimensional materials, microorganisms, and the immune system, *Adv. Drug Delivery Rev.*, 2022, **188**, 114422.
8 A. N. Ghulam, O. A. L. Dos Santos, L. Hazeem, B. Pizzorno Backx, M. Bououdina and S. Bellucci, Graphene Oxide (GO) Materials-Applications and Toxicity on Living Organisms and Environment, *J. Funct. Biomater.*, 2022, **13**(2), 77.
9 N. Malhotra, O. B. Villaflores, G. Audira, P. Siregar, J. S. Lee and T. R. Ger, *et al.*, Toxicity Studies on Graphene-Based Nanomaterials in Aquatic Organisms: Current Understanding, *Molecules*, 2020, **25**(16), 3618.
10 Y. Xuan, W. Zhang, X. Zhu and S. Zhang, An updated overview of some factors that influence the biological effects of nanoparticles, *Front. Bioeng. Biotechnol.*, 2023, **11**, 1254861.
11 J. Li, H. Zeng, Z. Zeng, Y. Zeng and T. Xie, Promising Graphene-Based Nanomaterials and Their Biomedical Applications and Potential Risks: A Comprehensive Review, *ACS Biomater. Sci. Eng.*, 2021, **7**(12), 5363–5396.
12 N. Ruijter, L. G. Soeteman-Hernandez, M. Carriere, M. Boyles, P. McLean and J. Catalan, *et al.*, The State of the Art and Challenges of In Vitro Methods for Human Hazard Assessment of Nanomaterials in the Context of Safe-by-Design, *Nanomaterials*, 2023, **13**(3), 472.
13 M. Adhish and I. Manjubala, Effectiveness of zebrafish models in understanding human diseases—A review of models, *Heliyon*, 2023, **9**(3), e14557.
14 M. Rocha, N. Singh, K. Ahsan, A. Beiriger and V. E. Prince, Neural crest development: insights from the zebrafish, *Dev. Dyn.*, 2020, **249**(1), 88–111.
15 W. Zhao, Y. Chen, N. Hu, D. Long and Y. Cao, The uses of zebrafish (Danio rerio) as an in vivo model for toxicological studies: A review based on bibliometrics, *Ecotoxicol. Environ. Saf.*, 2024, **272**, 116023.
16 X. Fan, T. Hou, S. Zhang, Y. Guan, J. Jia and Z. Wang, The cellular responses of autophagy, apoptosis, and 5-methylcytosine level in zebrafish cells upon nutrient deprivation stress, *Chemosphere*, 2020, **241**, 124989.
17 E. Haque and A. C. Ward, Zebrafish as a Model to Evaluate Nanoparticle Toxicity, *Nanomaterials*, 2018, **8**(7), 561.
18 Innovation R., Safe and sustainable by design: European Commission 2024 [cited 14/12/124], available from: **https://research-and-innovation.ec.europa.eu/research-area/**

industrial-research-and-innovation/chemicals-and-advanced-materials/safe-and-sustainable-design_en.

19 C. Apel, K. Kümmerer, A. Sudheshwar, B. Nowack, C. Som and C. Colin, *et al.*, Safe-and-sustainable-by-design: State of the art approaches and lessons learned from value chain perspectives. Current Opinion in Green and Sustainable, *Chemistry*, 2024, **45**, 100876.

20 S. Kumuda, U. Gandhi, U. Mangalanathan and K. Rajanna, Synthesis and characterization of graphene oxide and reduced graphene oxide chemically reduced at different time duration, *J. Mater. Sci.: Mater. Electron.*, 2024, **35**(9), 1.

21 Y. Park, J. Y. Koo, S. Kim and H. C. Choi, Spontaneous Formation of Gold Nanoparticles on Graphene by Galvanic Reaction through Graphene, *ACS Omega*, 2019, **4**(19), 18423–18427.

22 B. Ibrahim, T. H. Akere, S. Chakraborty, E. Valsami-Jones and H. Ali-Boucetta, Functionalized Gold Nanoparticles Suppress the Proliferation of Human Lung Alveolar Adenocarcinoma Cells by Deubiquitinating Enzymes Inhibition, *ACS Omega*, 2023, **8**(43), 40622–40638.

23 B. Ibrahim, T. H. Akere, S. Chakraborty, E. Valsami-Jones and H. Ali-Boucetta, Modulation of Heat Shock Protein Expression in Alveolar Adenocarcinoma Cells through Gold Nanoparticles and Cisplatin Treatment, *Pharmaceutics*, 2024, **16**(3), 380.

24 B. Ibrahim, T. H. Akere, S. Chakraborty, E. Valsami-Jones and H. Ali-Boucetta, Gold Nanoparticles Induced Size Dependent Cytotoxicity on Human Alveolar Adenocarcinoma Cells by Inhibiting the Ubiquitin Proteasome System, *Pharmaceutics*, 2023, **15**(2), 432.

25 A. Sánchez-Cepeda, E. Cedeño, E. Marín, M. C. Pazos, S.-C. Ingrid and E. J. Muñoz, *et al.*, Evaluation of the dispersion properties of graphene oxide/cetyltrimethylammonium bromide for application in nanocomposite materials, *RSC Adv.*, 2024, **14**(5), 3267–3279.

26 L. S. Franqui, M. A. De Farias, R. V. Portugal, C. A. R. Costa, R. R. Domingues and A. G. Souza Filho, *et al.*, Interaction of graphene oxide with cell culture medium: Evaluating the fetal bovine serum protein corona formation towards in vitro nanotoxicity assessment and nanobiointeractions, *Mater. Sci. Eng., C*, 2019, **100**, 363–377.

27 Z. Xu, Y. Gan, J. Zeng, J. Chen, A. Fu and X. Zheng, *et al.*, Green synthesis of functionalized fluorescent carbon dots from biomass and their corrosion inhibition mechanism for copper in sulfuric acid environment, *Chem. Eng. J.*, 2023, **470**, 144425.

28 L. Xuan, Z. Ju, M. Skonieczna, P. K. Zhou and R. Huang, Nanoparticles-induced potential toxicity on human health: Applications, toxicity mechanisms, and evaluation models, *MedComm*, 2023, **4**(4), e327.

29 L. H. Chen, H. T. Shen, W. H. Chang, I. Khalil, S. Y. Liao and W. A. Yehye, *et al.*, Photocatalytic Properties of Graphene/Gold and Graphene Oxide/Gold Nanocomposites Synthesized by Pulsed Laser Induced Photolysis, *Nanomaterials*, 2020, **10**(10), 1985.

30 Z. Ayreen, U. Khatoon, A. Kirti, A. Sinha, A. Gupta and S. S. Lenka, *et al.*, Perilous paradigm of graphene oxide and its derivatives in biomedical applications: Insight to immunocompatibility, *Biomed. Pharmacother.*, 2024, **176**, 116842.

31 P. Huang, C. Wang, H. Deng, Y. Zhou and X. Chen, Surface Engineering of Nanoparticles toward Cancer Theranostics, *Acc. Chem. Res.*, 2023, **56**(13), 1766–1779.

32 L. E. Gonzalez-Garcia, M. N. MacGregor, R. M. Visalakshan, A. Lazarian, A. A. Cavallaro and S. Morsbach, *et al.*, Nanoparticles Surface Chemistry Influence on Protein Corona Composition and Inflammatory Responses, *Nanomaterials*, 2022, **12**(4), 682.

33 S. Mazumdar, D. Chitkara and A. Mittal, Exploration and insights into the cellular internalization and intracellular fate of amphiphilic polymeric nanocarriers, *Acta Pharm. Sin. B*, 2021, **11**(4), 903–924.

34 M. Mehta, T. A. Bui, X. Yang, Y. Aksoy, E. M. Goldys and W. Deng, Lipid-Based Nanoparticles for Drug/Gene Delivery: An Overview of the Production Techniques and Difficulties Encountered in Their Industrial Development, *ACS Mater. Au*, 2023, **3**(6), 600–619.

35 A. Quevedo, L.-J. Ellis, I. Lynch and E. Valsami-Jones, Mechanisms of Silver Nanoparticle Uptake by Embryonic Zebrafish Cells, *Nanomaterials*, 2021, **11**(10), 2699.

36 A. C. Quevedo, I. Lynch and E. Valsami-Jones, Silver nanoparticle induced toxicity and cell death mechanisms in embryonic zebrafish cells, *Nanoscale*, 2021, **13**(12), 6142–6161.

37 E. Fleurbaix, M. Parant, A. Maul and C. Cossu-Leguille, Toxicity of lanthanides on various fish cell lines, *Ecotoxicology*, 2022, **31**(7), 1147–1157.

38 J. Ali, Y. Li, E. Shang, X. Wang, J. Zhao and M. Mohiuddin, *et al.*, Aggregation of graphene oxide and its environmental implications in the aquatic environment, *Chin. Chem. Lett.*, 2023, **34**(2), 107327.

39 A. Rauf, A. A. Khalil, S. Awadallah, S. A. Khan, T. Abu-Izneid and M. Kamran, *et al.*, Reactive oxygen species in biological systems: Pathways, associated diseases, and potential inhibitors—A review, *Food Sci. Nutr.*, 2023, **12**, 675–693.

40 W. Guo, Y. Xing, X. Luo, F. Li, M. Ren and Y. Liang, Reactive Oxygen Species: A Crosslink between Plant and Human Eukaryotic Cell Systems, *Int. J. Mol. Sci.*, 2023, **24**(17), 13052.

41 H. M. Abuzeid, C. M. Julien, L. Zhu and A. M. Hashem, Green Synthesis of Nanoparticles and Their Energy Storage, Environmental, and Biomedical Applications, *Crystals*, 2023, **13**(11), 1576.

42 X. Tong, R. Tang, M. Xiao, J. Xu, W. Wang and B. Zhang, *et al.*, Targeting cell death pathways for cancer therapy: recent developments in necroptosis, pyroptosis, ferroptosis, and cuproptosis research, *J. Hematol. Oncol.*, 2022, **15**(1), 174.

43 A. Taheriazam, G. G. Y. Abad, S. Hajimazdarany, M. H. Imani, S. Ziaolhagh and M. A. Zandieh, *et al.*, Graphene oxide nanoarchitectures in cancer biology: Nano-modulators of autophagy and apoptosis, *J. Controlled Release*, 2023, **354**, 503–522.

44 H. S. Hsieh and R. G. Zepp, Reactivity of graphene oxide with reactive oxygen species (hydroxyl radical, singlet oxygen, and superoxide anion), *Environ. Sci.: Nano*, 2019, **6**(12), 3734–3744.

45 E. Maldonado, S. Morales-Pison, F. Urbina and A. Solari, Aging Hallmarks and the Role of Oxidative Stress, *Antioxidants*, 2023, **12**(3), 651.